Design of three-dimensional nonlinear guidance law with bounded acceleration command

Runle Du [a], Kezi Meng [b,*], Di Zhou [b], Jiaqi Liu [a]

[a] *National Key Laboratory of Science and Technology on Test Physics & Numerical Mathematics, 100076 Beijing, PR China*
[b] *School of Astronautics, Harbin Institute of Technology, 150001 Harbin, PR China*

ABSTRACT

This paper concentrates on the problem of designing a three-dimensional nonlinear guidance law accounting for saturation nonlinearity and the dynamics of missile autopilot based on a command filtered backstepping (CFBS) scheme. In the design, the nonlinear kinematics of target–missile engagement is considered in the spherical coordinate system and the dynamics of the autopilot is considered as a second-order term. The CFBS scheme is utilized to blend the command filtering approach into standard backstepping method to avoid the complex computation of the analytic derivatives of the intermediate control signals. A command filter with a saturation limiter embedded and some auxiliary filters are combined together to address acceleration command saturation. Simulation results show that even though subject to saturation constraint, the proposed guidance law achieves excellent guidance performance in terms of missed distance.

1. Introduction

The main mission of a missile terminal guidance law is to specify acceleration commands to the missile's autopilot such that the missile produces a minimum miss distance with respect to its target [22]. Proportional navigation (PN) guidance law [28] has obtained widespread applications because of its simplicity and easy implementation. Also, the effectiveness of PN guidance law is fully exhibited in guiding missiles to intercept non-maneuvering or weakly maneuvering targets. However, when used for intercepting highly maneuvering and agile targets in the modern wars, PN guidance law may fail to meet the desired precision requirement. The augmented proportional navigation (APN) guidance law [28] modified from PN guidance law can cope with target maneuvers well. Nevertheless, it needs accurate target acceleration information which is often unknown or poorly estimated in practical applications. To deal with highly maneuvering and agile targets in the absence of its acceleration, some new guidance laws based on nonlinear control method and robust control method have been proposed, such as Lyapunov-based nonlinear guidance laws [20,12,26], nonlinear geometric guidance laws [1,27], differential game guidance laws [19,29], nonlinear H_∞ guidance laws [24,25], L_2 gain guidance law [31], and sliding-mode guidance laws

[32,14,30,13,10]. However, in the design of these guidance laws, the closed-loop contour of an auto-piloted missile, normally briefly called missile autopilot, is treated as an ideal term.

In practice, for endo-atmospheric missiles, the dynamics of missile autopilot usually exerts a bad influence on guidance precision, especially in the presence of target maneuvers. Thus, it is necessary to consider the dynamics of missile autopilot in the design of guidance laws. Actually, the autopilot of a missile is of high-order dynamics [16], but for the purpose of designing a guidance law, it can be greatly approximated. The most simple approximation of the dynamics of missile autopilot is a first-order lag. Considering the missile autopilot as a first-order lag, Golestani et al. [5] and Sun et al. [23] designed some guidance laws with finite time convergence using backstepping method, and Hexner and Weiss [9] proposed a stochastic optimal guidance law with significant uncertainty. However, for agile missiles, the transient performance of autopilot cannot be well approximated by the first order lag because of its property of none overshoot and slow rising rate. Actually, the dynamics of missile autopilot can be better approximated as a second-order oscillatory term. With such an approximation, Chwa and Choi [2] proposed an adaptive sliding-mode nonlinear guidance law, and Zhou and Qu [33] designed a guidance law with terminal impact angle constraint using dynamic surface control.

In practical applications, besides the influence of the dynamics of missile autopilot, missile acceleration saturation is another factor normally encountered in the design of missile guidance law, especially when the target's maneuverability is close to that of

* Corresponding author. Tel.: +8 615590860792.
E-mail address: ljymkz@126.com (K. Meng).

Nomenclature

CFBS   Command filtered backstepping
CFBSG   CFBS-based guidance
LOS   Line-of-sight
a_i $(i = 1, \ldots, 5)$ Dynamic coefficients
$a_{Mr}, a_{M\theta}, a_{M\phi}$ Components of missile acceleration along LOS axes
$a_{Tr}, a_{T\theta}, a_{T\phi}$ Components of target acceleration along LOS axes
$\|a_{T\theta}\|_\infty, \|a_{T\phi}\|_\infty$ Suprema of $a_{T\theta}$ and $a_{T\phi}$.
$\boldsymbol{e}_r, \boldsymbol{e}_\theta, \boldsymbol{e}_\phi$ Unit vectors along the spherical coordinate axes
g Gravity acceleration
$G_1(s)$ Transfer function from angle of rudder reflection to body's angular rate
$G_2(s)$ Transfer function from angle of rudder reflection to acceleration output
$G_a(s)$ Transfer function of the accelerometer
$G_d(s)$ Transfer function of the rudder
$G_g(s)$ Transfer function of the gyroscope
r Target–missile relative range
u_{ic}^0 $(i = \theta, \phi)$ Nominal controls
u_{ic} $(i = \theta, \phi)$ Filtered versions of nominal controls

u_θ, u_ϕ Acceleration commands to be designed corresponding to $a_{M\theta}$ and $a_{M\phi}$
V Velocity of the missile
x_j $(j = 1, \ldots, 6)$ Defined state variables
x_{jc} $(j = 1, \ldots, 6)$ Desired values of state variables
x_{jc}^0 $(j = 3, \ldots, 6)$ Intermediate virtual controls
x_{jc} $(j = 3, \ldots, 6)$ Filtered versions of intermediate virtual controls
$\tilde{x}_j$ $(j = 1, \ldots, 6)$ Tracking errors
δ Angle of rudder reflection
ϕ LOS elevation angle
μ Upper bound of u_i $(i = \theta, \phi)$
θ LOS azimuth angle
ς_i $(i = 1, \ldots, 6)$ Auxiliary filter variables to characterize the effect of the errors $x_{jc} - x_{jc}^0$ $(j = 3, \ldots, 6)$ and $u_{ic} - u_{ic}^0$ $(i = \theta, \phi)$ on tracking errors $\tilde{x}_j$ $(j = 1, \ldots, 6)$
ω Body's angular rate
ω_n Natural oscillation frequency of missile autopilot
ζ Damping ratio of missile autopilot

the homing missile. If a guidance law is designed without considering acceleration command constraint, it may cause a severe deterioration of the guidance performance and even the instability of the guidance system, leading to the failure of the interception. Therefore, it is quite significant to investigate missile guidance laws with bounded acceleration command. Up to now, researchers on this topic have mainly focused on utilizing optimal control methods [17,18,15,7,8,6]. For example, deterministic formulas of optimal guidance law for acceleration constrained missile were derived from the missile's transfer function via directly minimizing the Hamilton function subject to constrained control to satisfy a quadratic objective [17,18]. Furthermore, the formulas were extended to the case of random maneuvering targets and noisy measurements [15]. Moreover, a stochastic optimal guidance law numerically solved dependent on conditional probability density function of the estimated states for a missile with bounded acceleration was presented [7] and then a linear approximation of the guidance law was derived using random-input describing function (RIDF) [8]. A stochastic optimal guidance law accounting for constraints on both missile acceleration command and guidance gain was synthesized using the linear quadratic stochastic Gaussian optimal control theory and RIDF [6].

The preceding guidance laws with bounded acceleration were designed based on ideal missile autopilot and simplified engagement dynamics in terms of linear target–missile relative range and relative velocity in the reference Cartesian coordinate system. It is well known that guidance laws steering the line-of-sight (LOS) angular rate are apt to be realized in practical applications. However, the relative motion model described in the spherical coordinate system must be nonlinear equations. This brings some difficulties to the design of guidance law. To the best of our knowledge, it has not been investigated to design a guidance law accounting for both the acceleration command constraint and the second-order dynamics of missile autopilot under the nonlinear kinematics of target–missile engagement. In this paper, we will address this problem by applying the command filtered backstepping scheme (CFBS) [3] to the design of guidance law. The CFBS has been applied to the design of nonlinear flight control law [4,21], but this is its first application to the design of guidance law. The command filters in the CFBS scheme obviate the need for computing analytic derivatives in standard backstepping. A saturation limiter is
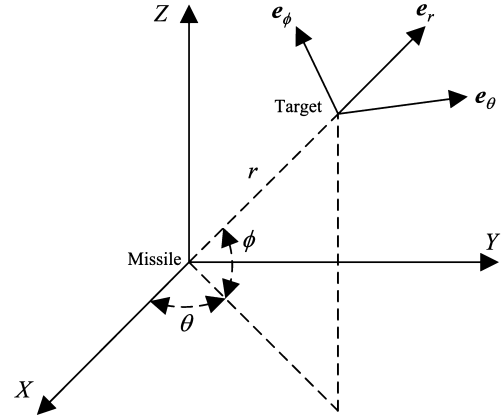

Fig. 1. Target–missile engagement geometry in three-dimensional space.

embedded into the command filter to enforce the constraints on guidance commands and an auxiliary error compensation is employed to eliminate the effect of the constraints.

The rest of this paper is organized as follows. In Section 2, the three-dimensional nonlinear kinematics of target–missile engagement and the second-order dynamics of the missile autopilot are presented. The design procedure of the guidance law based on CFBS scheme are formulated in Section 3. Simulation results are provided in Section 4 to verify the effectiveness of the proposed guidance law. Some concluding remarks are made in Section 5.

2. Formulation of target–missile engagement

Consider three-dimensional target–missile engagement geometry in the spherical coordinate system (r, θ, ϕ), as shown in Fig. 1. By virtue of the principles of kinematics, the three relative acceleration components can be expressed by the following set of second-order nonlinear differential equations [25]:

$$\ddot{r} - r\dot{\phi}^2 - r\dot{\theta}^2 \cos^2\phi = a_{Tr} - a_{Mr} \tag{1a}$$

$$r\ddot{\theta}\cos\phi + 2\dot{r}\dot{\theta}\cos\phi - 2r\dot{\phi}\dot{\theta}\sin\phi = a_{T\theta} - a_{M\theta} \tag{1b}$$

$$r\ddot{\phi} + 2\dot{r}\dot{\phi} + r\dot{\theta}^2 \sin\phi\cos\phi = a_{T\phi} - a_{M\phi} \tag{1c}$$
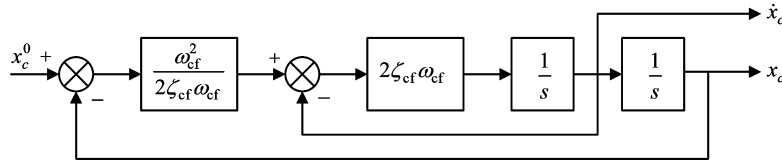
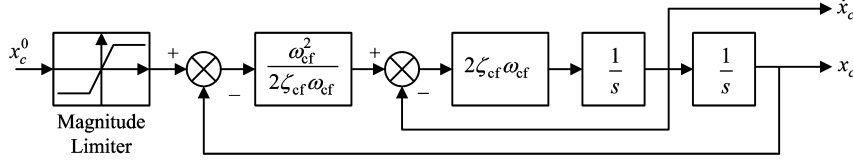**Fig. 2.** Block diagram of command filter.

Fig. 3. Block diagram of command filter with magnitude limiter.

In general, during the process of terminal guidance, only the accelerations normal to LOS, i.e. $a_{M\theta}$ and $a_{M\phi}$, are adjustable. Under the premise that the target–missile radial relative velocity $\dot{r}$ is negative, the objective of designing a guidance law is to determine $a_{M\theta}$ and $a_{M\phi}$ to nullify LOS angular rates $\dot{\theta}$ and $\dot{\phi}$. Therefore, only LOS angular motion equations (1b) and (1c) are used for the design of the guidance law.

Furthermore, we assume that the closed-loop contour of the auto-pilot missile can be approximated as second-order dynamics which are given as follows:

$$\begin{cases} \ddot{a}_{M\theta} = -2\zeta\omega_n\dot{a}_{M\theta} - \omega_n^2 a_{M\theta} + \omega_n^2 sat(u_\theta) \\ \ddot{a}_{M\phi} = -2\zeta\omega_n\dot{a}_{M\phi} - \omega_n^2 a_{M\phi} + \omega_n^2 sat(u_\phi) \end{cases} \quad (2)$$

where

$$sat(u_i) = \begin{cases} \mu & \text{if } u_i > \mu \\ u_i & \text{if } |u_i| \le \mu, \ i = \theta, \phi \\ -\mu & \text{if } u_i < -\mu \end{cases}$$

Define state variables as $x_1 = \dot{\theta}$, $x_2 = \dot{\phi}$, $x_3 = a_{M\theta}$, $x_4 = a_{M\phi}$, $x_5 = \dot{a}_{M\theta}$, and $x_6 = \dot{a}_{M\phi}$ and control variables as u_θ and u_ϕ. Then, Eqs. (1b), (1c), and (2) are rewritten in the following state-space form:

$$\begin{cases} \dot{x}_1 = -\dfrac{2\dot{r}}{r}x_1 + 2x_1 x_2 \tan\phi - \dfrac{x_3}{r\cos\phi} + \dfrac{a_{T\theta}}{r\cos\phi} \\ \dot{x}_2 = -\dfrac{2\dot{r}}{r}x_2 - x_1^2 \sin\phi\cos\phi - \dfrac{x_4}{r} + \dfrac{a_{T\phi}}{r} \\ \dot{x}_3 = x_5 \\ \dot{x}_4 = x_6 \\ \dot{x}_5 = -2\zeta\omega_n x_5 - \omega_n^2 x_3 + \omega_n^2 sat(u_\theta) \\ \dot{x}_6 = -2\zeta\omega_n x_6 - \omega_n^2 x_4 + \omega_n^2 sat(u_\phi) \end{cases} \quad (3)$$

3. CFBS-based guidance law

In this section, the command filters involved in the CFBS scheme are presented first, and then the design procedure of CFBS-based guidance law is elaborated.

3.1. Command filter

The block diagram of the command filter is depicted in Fig. 2. The signal x_c is the command filtered version of the input signal x_c^0 and $\dot{x}_c$ is time derivative of signal x_c. The design parameters of this filter are $\omega_{cf} > 0$ and $\zeta_{cf} > 0$.

The state-space representation of the command filter is

$$\begin{cases} \begin{bmatrix} \dot{q}_1 \\ \dot{q}_2 \end{bmatrix} = \begin{bmatrix} 0 & 1 \\ -\omega_{cf}^2 & -2\zeta_{cf}\omega_{cf} \end{bmatrix} \begin{bmatrix} q_1 \\ q_2 \end{bmatrix} + \begin{bmatrix} 0 \\ \omega_{cf}^2 \end{bmatrix} x_c^0 \\ \begin{bmatrix} x_c \\ \dot{x}_c \end{bmatrix} = \begin{bmatrix} q_1 \\ q_2 \end{bmatrix} \end{cases} \quad (4a)$$

To impose saturation constraint on acceleration command, as shown in Fig. 3, a saturation limiter is embedded into the command filter to form the command filter with magnitude limiter.

The state-space form of command filter with magnitude limiter can be expressed as

$$\begin{cases} \begin{bmatrix} \dot{q}_1 \\ \dot{q}_2 \end{bmatrix} = \begin{bmatrix} q_2 \\ 2\zeta_{cf}\omega_{cf}[\dfrac{\omega_{cf}^2}{2\zeta_{cf}\omega_{cf}}(sat(x_c^0) - q_1) - q_2] \end{bmatrix} \\ \begin{bmatrix} x_c \\ \dot{x}_c \end{bmatrix} = \begin{bmatrix} q_1 \\ q_2 \end{bmatrix} \end{cases} \quad (4b)$$

3.2. Design procedure of CFBS-based guidance law

In this section, we will adopt CFBS scheme to design a guidance law which incorporates acceleration command saturation and the dynamics of missile autopilot.

Define the tracking errors as

$$\tilde{x}_j = x_j - x_{jc}, \quad j = 1, 2, \ldots, 6 \quad (5)$$

where $x_{1c} = 0$ and $x_{2c} = 0$ are the desired values of $\dot{\theta}$ and $\dot{\phi}$, respectively.

Consider x_3 and x_4 as the virtual controls and find desired virtual control laws α_1 and α_2 that stabilize $\tilde{x}_1$ and $\tilde{x}_2$ by using the following control Lyapunov function:

$$V_1 = \frac{1}{2}\tilde{x}_1^2 + \frac{1}{2}\tilde{x}_2^2 \quad (6)$$

To render the time derivative of V_1 along the trajectories of the system of Eq. (3) under α_1 and α_2 to be negative definite, i.e.,

$$\dot{V}_1 = \tilde{x}_1\left(-\frac{2\dot{r}}{r}x_1 + 2x_1 x_2 \tan\phi - \frac{\alpha_1}{r\cos\phi} + \frac{a_{T\theta}}{r\cos\phi} - \dot{x}_{1c}\right)$$
$$+ \tilde{x}_2\left(-\frac{2\dot{r}}{r}x_2 - x_1^2 \sin\phi\cos\phi - \frac{\alpha_2}{r} + \frac{a_{T\phi}}{r} - \dot{x}_{2c}\right) < 0,$$
$$\tilde{x}_1 \ne 0, \ \tilde{x}_2 \ne 0 \quad (7)$$

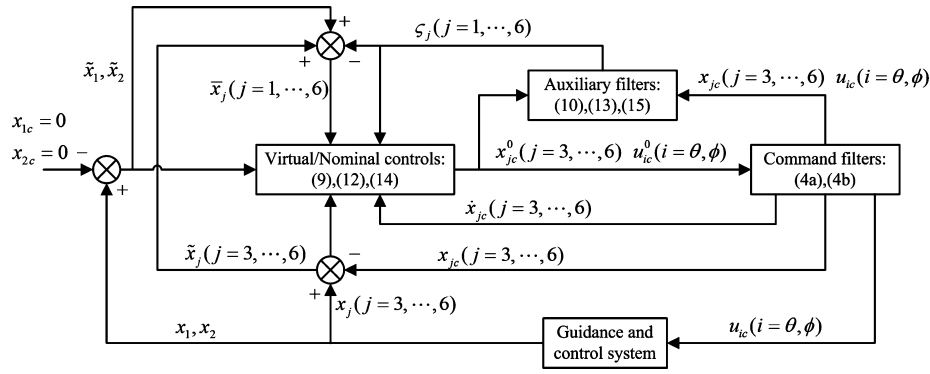**Fig. 4.** CFBS-based guidance scheme.

the virtual control laws α_1 and α_2 are selected as

$$\begin{cases} \alpha_1 = r\cos\phi \left(\begin{array}{c} k_1\tilde{x}_1 - \dfrac{2\dot{r}}{r}x_1 + \\ 2x_1 x_2 \tan\phi - \dot{x}_{1c} \end{array} \right) + \varepsilon_1 \mathrm{sgn}\tilde{x}_1 \\[4mm] \alpha_2 = r \left(\begin{array}{c} k_2\tilde{x}_2 - \dfrac{2\dot{r}}{r}x_2 - \\ x_1^2 \sin\phi\cos\phi - \dot{x}_{2c} \end{array} \right) + \varepsilon_2 \mathrm{sgn}\tilde{x}_2 \end{cases} \tag{8}$$

where $k_1 = \mathrm{const.} > 0$, $k_2 = \mathrm{const.} > 0$, $\varepsilon_1 = \mathrm{const.} > \|a_{T\theta}\|_\infty$, and $\varepsilon_2 = \mathrm{const.} > \|a_{T\phi}\|_\infty$.

To handle saturation constraints imposed on the acceleration commands, the remaining design steps are formulated as follows.

Step 1) Define

$$\begin{cases} x_{3c}^0 = \alpha_1 - \varsigma_3 \\ x_{4c}^0 = \alpha_2 - \varsigma_4 \end{cases} \tag{9}$$

where ς_3 and ς_4 will be defined in step 3).

Let the virtual controls x_{3c}^0 and x_{4c}^0 go through the command filter denoted by Eq. (4a) to produce x_{3c} and x_{4c} as well as their derivatives $\dot{x}_{3c}$ and $\dot{x}_{4c}$, respectively. Then implement the following two filters:

$$\begin{cases} \dot{\varsigma}_1 = -k_1\varsigma_1 - \dfrac{1}{r\cos\phi}(x_{3c} - x_{3c}^0), & \varsigma_1(0) = 0 \\[3mm] \dot{\varsigma}_2 = -k_2\varsigma_2 - \dfrac{1}{r}(x_{4c} - x_{4c}^0), & \varsigma_2(0) = 0 \end{cases} \tag{10}$$

to estimate ς_1 and ς_2.

Step 2) Define the compensated tracking errors as

$$\bar{x}_j = \tilde{x}_j - \varsigma_j, \quad j = 1, 2, \ldots, 6 \tag{11}$$

Step 3) Define

$$\begin{cases} x_{5c}^0 = -k_3\tilde{x}_3 + \dot{x}_{3c} + \dfrac{1}{r\cos\phi}\bar{x}_1 - \varsigma_5 \\[3mm] x_{6c}^0 = -k_4\tilde{x}_4 + \dot{x}_{4c} + \dfrac{1}{r}\bar{x}_2 - \varsigma_6 \end{cases} \tag{12}$$

where $k_3 = \mathrm{const.} > 0$ and $k_4 = \mathrm{const.} > 0$. ς_5 and ς_6 will be defined in step 4).

Let the virtual controls x_{5c}^0 and x_{6c}^0 go through command filter denoted by Eq. (4a) to produce x_{5c} and x_{6c} as well as their derivatives $\dot{x}_{5c}$ and $\dot{x}_{6c}$, respectively. Further, implement the following two filters to compute ς_3 and ς_4 which are involved in Eq. (9):

$$\begin{cases} \dot{\varsigma}_3 = -k_3\varsigma_3 + (x_{5c} - x_{5c}^0), \ \varsigma_3(0) = 0 \\ \dot{\varsigma}_4 = -k_4\varsigma_4 + (x_{6c} - x_{6c}^0), \ \varsigma_4(0) = 0 \end{cases} \tag{13}$$

Step 4) Define the nominal controls as

$$\begin{cases} u_{\theta c}^0 = \dfrac{1}{\omega_n^2}(-k_5\tilde{x}_5 + \dot{x}_{5c} + 2\zeta\omega_n x_5 + \omega_n^2 x_3 - \bar{x}_3) \\[3mm] u_{\phi c}^0 = \dfrac{1}{\omega_n^2}(-k_6\tilde{x}_6 + \dot{x}_{6c} + 2\zeta\omega_n x_6 + \omega_n^2 x_4 - \bar{x}_4) \end{cases} \tag{14}$$

where $k_5 = \mathrm{const.} > 0$, $k_6 = \mathrm{const.} > 0$.

Through the command filter with the magnitude limiter, Eq. (4b), nominal controls $u_{\theta c}^0$ and $u_{\phi c}^0$ are filtered to produce magnitude-limited controls $u_{\theta c}$ and $u_{\phi c}$. Similarly, the effect on tracking errors $\tilde{x}_5$ and $\tilde{x}_6$ resulting from the difference between the achievable control signals ($u_{\theta c}$ and $u_{\phi c}$) and the desired control signals ($u_{\theta c}^0$ and $u_{\phi c}^0$) are estimated by implementing the following two filters:

$$\begin{cases} \dot{\varsigma}_5 = -k_5\varsigma_5 + \omega_n^2(u_{\theta c} - u_{\theta c}^0), & \varsigma_5(0) = 0 \\ \dot{\varsigma}_6 = -k_6\varsigma_6 + \omega_n^2(u_{\phi c} - u_{\phi c}^0), & \varsigma_6(0) = 0 \end{cases} \tag{15}$$

The main differences between u_{ic} ($i = \theta, \phi$) and u_{ic}^0 ($i = \theta, \phi$) are originated from saturation constraint. By virtue of the command filter with magnitude constraint, $u_{\theta c}$ and $u_{\phi c}$ are necessarily within the magnitude limits of u_θ and u_ϕ, respectively. Consequently, they are implementable physically. We therefore set

$$sat(u_\theta) = u_{\theta c}, \qquad sat(u_\phi) = u_{\phi c} \tag{16}$$

The specified CFBS-based guidance scheme is shown in Fig. 4. In spite of the complex form, the CFBS-based guidance is not hard to solve because the differential equations included in it are all low-order and linear. The differential equations can be easily solved by 4-order Runge–Kutta algorithm. The time consumed on solving one-step acceleration command is only 10 ms using Matlab programming in an ordinary computer. Also, in consideration of the rapid calculation ability of modern computers, the CFBS-based guidance is not difficult to implement using DSP onboard the missile.

Theorem 1. *For guidance system (3), the CFBS-based guidance law including Eqs. (8)–(16) can guarantee that the compensated tracking errors $\bar{x}_j$ ($j = 1, \ldots, 6$) defined in Eq. (11) converge to zero exponentially as time approaches infinity.*

Proof. Note that x_{jc}^0 ($j = 3, 4$) are filtered through the command filter Eq. (4a) rather than the command filter with magnitude limiter Eq. (4b), because they don't suffer from saturation. Thus, the errors $|x_{jc} - x_{jc}^0|$ ($j = 3, 4$) can be made arbitrarily small by selecting a sufficiently large parameter ω_{cf}, then $\varsigma_1 \to 0$, $\varsigma_2 \to 0$ by Eq. (10), implying $\tilde{x}_1 \to \bar{x}_1$, $\tilde{x}_2 \to \bar{x}_2$. So we replace $\tilde{x}_1$ and $\tilde{x}_2$ in Eq. (8) with $\bar{x}_1$ and $\bar{x}_2$, respectively, i.e.,

$$\begin{cases} \alpha_1 = r\cos\phi \begin{pmatrix} k_1\tilde{x}_1 - \dfrac{2\dot{r}}{r}x_1 + \\ 2x_1x_2\tan\phi - \dot{x}_{1c} \end{pmatrix} + \varepsilon_1\mathrm{sgn}\bar{x}_1 \\[12pt] \alpha_2 = r \begin{pmatrix} k_2\tilde{x}_2 - \dfrac{2\dot{r}}{r}x_2 - \\ x_1^2\sin\phi\cos\phi - \dot{x}_{2c} \end{pmatrix} + \varepsilon_2\mathrm{sgn}\bar{x}_2 \end{cases} \tag{17}$$

After some algebraic manipulation, the dynamics of the tracking errors $\tilde{x}_j$ ($j = 1, \ldots, 6$) can be written as

$$\dot{\tilde{x}}_1 = -\frac{2\dot{r}}{r}x_1 + 2x_1x_2\tan\phi - \frac{1}{r\cos\phi}x_{3c}^0$$
$$- \frac{1}{r\cos\phi}\left(x_{3c} - x_{3c}^0\right) - \frac{1}{r\cos\phi}(x_3 - x_{3c})$$
$$+ \frac{a_{T\theta}}{r\cos\phi} - \dot{x}_{1c} \tag{18a}$$

$$\dot{\tilde{x}}_2 = -\frac{2\dot{r}}{r}x_2 - x_1^2\sin\phi\cos\phi - \frac{1}{r}x_{4c}^0$$
$$- \frac{1}{r}\left(x_{4c} - x_{4c}^0\right) - \frac{1}{r}(x_4 - x_{4c})$$
$$+ \frac{a_{T\phi}}{r} - \dot{x}_{2c} \tag{18b}$$

$$\dot{\tilde{x}}_3 = x_{5c}^0 + \left(x_{5c} - x_{5c}^0\right) + (x_5 - x_{5c}) - \dot{x}_{3c} \tag{18c}$$

$$\dot{\tilde{x}}_4 = x_{6c}^0 + \left(x_{6c} - x_{6c}^0\right) + (x_6 - x_{6c}) - \dot{x}_{4c} \tag{18d}$$

$$\dot{\tilde{x}}_5 = -2\zeta\omega_n x_5 - \omega_n^2 x_3 + \omega_n^2 u_{\theta c}^0$$
$$+ \omega_n^2\left(u_{\theta c} - u_{\theta c}^0\right) - \dot{x}_{5c} \tag{18e}$$

$$\dot{\tilde{x}}_6 = -2\zeta\omega_n x_6 - \omega_n^2 x_4 + \omega_n^2 u_{\phi c}^0$$
$$+ \omega_n^2\left(u_{\phi c} - u_{\phi c}^0\right) - \dot{x}_{6c} \tag{18f}$$

Substituting Eqs. (17), (9), (10), and (12)–(16) into Eq. (18)) and combining the error definitions of Eqs. (5) and (11), we have

$$\dot{\tilde{x}}_1 = -k_1\bar{x}_1 - \frac{\bar{x}_3}{r\cos\phi} + \frac{a_{T\theta}}{r\cos\phi}$$
$$- \frac{\varepsilon_1}{r\cos\phi}\mathrm{sgn}\bar{x}_1 + \dot{\varsigma}_1 \tag{19a}$$

$$\dot{\tilde{x}}_2 = -k_2\bar{x}_2 - \frac{\bar{x}_4}{r} + \frac{a_{T\phi}}{r} - \frac{\varepsilon_2}{r}\mathrm{sgn}\bar{x}_2 + \dot{\varsigma}_2 \tag{19b}$$

$$\dot{\tilde{x}}_3 = -k_3\bar{x}_3 + \frac{\bar{x}_1}{r\cos\phi} + \bar{x}_5 + \dot{\varsigma}_3 \tag{19c}$$

$$\dot{\tilde{x}}_4 = -k_4\bar{x}_4 + \frac{\bar{x}_2}{r} + \bar{x}_6 + \dot{\varsigma}_4 \tag{19d}$$

$$\dot{\tilde{x}}_5 = -k_5\bar{x}_5 - \bar{x}_3 + \dot{\varsigma}_5 \tag{19e}$$

$$\dot{\tilde{x}}_6 = -k_6\bar{x}_6 - \bar{x}_4 + \dot{\varsigma}_6 \tag{19f}$$

Combining the compensated tracking error definition of Eq. (11) with Eq. (19), the compensated tracking error dynamics for $\bar{x}_j$ ($j = 1, 2, \ldots, 6$) are achieved as

$$\dot{\bar{x}}_1 = -k_1\bar{x}_1 - \frac{\bar{x}_3}{r\cos\phi} + \frac{a_{T\theta}}{r\cos\phi} - \frac{\varepsilon_1}{r\cos\phi}\mathrm{sgn}\bar{x}_1 \tag{20a}$$

$$\dot{\bar{x}}_2 = -k_2\bar{x}_2 - \frac{\bar{x}_4}{r} + \frac{a_{T\phi}}{r} - \frac{\varepsilon_2}{r}\mathrm{sgn}\bar{x}_2 \tag{20b}$$

$$\dot{\bar{x}}_3 = -k_3\bar{x}_3 + \frac{\bar{x}_1}{r\cos\phi} + \bar{x}_5 \tag{20c}$$

$$\dot{\bar{x}}_4 = -k_4\bar{x}_4 + \frac{\bar{x}_2}{r} + \bar{x}_6 \tag{20d}$$

$$\dot{\bar{x}}_5 = -k_5\bar{x}_5 - \bar{x}_3 \tag{20e}$$

$$\dot{\bar{x}}_6 = -k_6\bar{x}_6 - \bar{x}_4 \tag{20f}$$

Define a Lyapunov function candidate on the compensated tracking errors $\bar{x}_j$ ($j = 1, 2, \ldots, 6$) as

$$V(t) = \frac{1}{2}\sum_{j=1}^{6}\bar{x}_j^2 \tag{21}$$

Differentiating $V(t)$ with respect to time along the system trajectories of Eq. (20) yields

$$\dot{V}(t) = -\sum_{j=1}^{6}k_j\bar{x}_j^2 + \frac{a_{T\theta}}{r\cos\phi}\bar{x}_1$$
$$- \frac{\varepsilon_1}{r\cos\phi}|\bar{x}_1| + \frac{a_{T\phi}}{r}\bar{x}_2 - \frac{\varepsilon_2}{r}|\bar{x}_2| \tag{22}$$

where r is always greater than zero and an appropriate inertial reference coordinate system can be established to ensure that the LOS elevation angle, ϕ, belongs to the set $(-\pi/2, \pi/2)$ during the terminal guidance process. Obviously, $r\cos\phi$ is always greater than zero. Thus, we can get

$$\dot{V}(t) \leq -\sum_{j=1}^{6}k_j\bar{x}_j^2 + \frac{1}{r\cos\phi}\left(|a_{T\theta}| - \varepsilon_1\right)|\bar{x}_1| + \frac{1}{r}\left(|a_{T\phi}| - \varepsilon_2\right)|\bar{x}_2|$$
$$\leq -\sum_{j=1}^{6}k_j\bar{x}_j^2 \leq -k\sum_{j=1}^{6}\bar{x}_j^2 = -2kV(t) \tag{23}$$

where $k = \min\{k_j, j = 1, 2, \ldots, 6\}$. Furthermore,

$$V(t) \leq V(0)\exp[-2kt]$$
$$\Rightarrow \quad V(t) \to 0, t \to \infty$$
$$\Rightarrow \quad \lim_{t\to\infty}\bar{x}_j = 0, \quad j = 1, \ldots, 6 \tag{24}$$

According to Theorem 4.10 in [11], the equilibrium point $\bar{x}_j$ ($j = 1, 2, \ldots, 6$) $= 0$ of the compensated tracking error system described by Eq. (20) is exponentially stable regardless of the nominal controls $u_{\theta c}^0$ and $u_{\phi c}^0$. □

Theorem 1 leaves open the question of the properties of tracking errors $\tilde{x}_1$ and $\tilde{x}_2$, which should be the key point. However, we obtained that $\tilde{x}_1 \to \bar{x}_1$, $\tilde{x}_2 \to \bar{x}_2$ from Eq. (17). Namely, both x_1 and x_2 can asymptotically converge to zero as $\bar{x}_1$ and $\bar{x}_2$ converge to zero, satisfying the design objective.

4. Numerical simulations

For notational convience, thereafter we denote the proposed CFBS-based guidance law as CFBSG. Numerical simulations will be performed to demonstrate the effectiveness of the CFBSG against a highly maneuvering target based on an actual missile autopilot
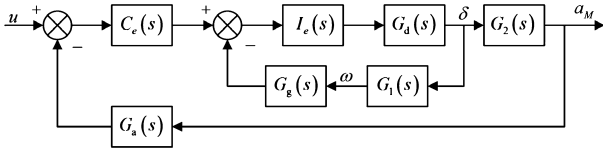
Fig. 5. Block diagram of actual missile autopilot.

model. Assume that a tail-controlled missile adopts pure aerodynamic control. The block diagram of the missile autopilot is as shown in Fig. 5.

In Fig. 5, u and a_M represent the acceleration command and the acceleration output, respectively. The transfer functions are given by

$$G_d(s) = \frac{\omega_d^2}{s^2 + 2\zeta_d\omega_d s + \omega_d^2} \tag{25}$$

$$G_g(s) = \frac{\omega_g^2}{s^2 + 2\zeta_g\omega_g s + \omega_g^2} \tag{26}$$

$$G_a(s) = \frac{\omega_a^2}{s^2 + 2\zeta_a\omega_a s + \omega_a^2} \tag{27}$$

$$G_1(s) = \frac{-a_3 s + a_2 a_5 - a_3 a_4}{s^2 + (a_1 + a_4)s + a_1 a_4 + a_2} \tag{28}$$

$$G_2(s) = \frac{V}{g}\frac{a_5 s^2 + a_1 a_5 s + a_2 a_5 - a_3 a_4}{s^2 + (a_1 + a_4)s + a_1 a_4 + a_2} \tag{29}$$

where $\zeta_d = 0.65$, $\omega_d = 120$, $\zeta_g = 0.4$, $\omega_g = 440.53$, $\zeta_a = 0.6$, and $\omega_a = 1129.94$. Also, the inner-loop and outer-loop adopt the body's angular rate feedback and acceleration feedback, respectively, and $I_e(s)$ and $C_e(s)$ represent controllers of the inner-loop and the outer-loop, respectively. Some typical characteristic points are chosen for designing the missile autopilot. For each characteristic points, the controllers $I_e(s)$ and $C_e(s)$ are designed using classical frequency domain method. For example, for a characteristic point at the altitude of 15 km where the dynamic coefficients are $a_1 = 0.162$, $a_2 = 0.7155$, $a_3 = 42.713$, $a_4 = 0.258$, and $a_5 = 0.042$, the inner-loop and outer-loop controllers are respectively designed as

$$I_e(s) = -0.35 \tag{30}$$

$$C_e(s) = \frac{0.08(1 + 1.3s)}{s(1 + 0.076s)} \tag{31}$$

Apparently, the dynamics of the missile autopilot from u to a_M must be a high-order and non-minimum phase term. In the design of guidance law, we approximate this term with the second-order dynamics.

Define an inertial reference coordinate system which is parallel to $MXYZ$ coordinate system in Fig. 1. It is inertially fixed and is centered at the missile launch point. In the coordinate system, X axis is along the direction of launch in the horizontal plane and Z axis is perpendicular to X axis and upward in the vertical plane, Y axis being established according to right-hand rule. The missile's initial position coordinates are $x_{M0} = 50$ km, $y_{M0} = 10$ km and $z_{M0} = 10$ km. Its initial velocity is $V_{M0} = 1000$ m/s and its initial flight-path and heading angles are $\theta_{M0} = 32.5°$ and $\psi_{VM0} = 2.4°$, respectively. The target's initial position coordinates are $x_{T0} = 80$ km, $y_{T0} = 20$ km and $z_{T0} = 18$ km. Its initial velocity is $V_{T0} = 1300$ m/s and its initial flight-path and heading angles are $\theta_{T0} = 2°$ and $\psi_{VT0} = 150°$, respectively. The acceleration command bound is $\mu = 7.5$ g. The maneuvers of the target are $a_{T\theta} = -70\sin(\pi t/3)$ m/s^2 and $a_{T\phi} = 70\sin(\pi t/3)$ m/s^2.

Table 1
Command filter parameters.

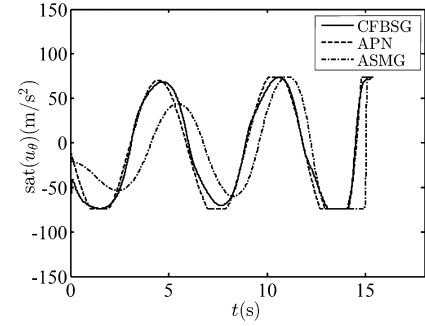| Command variable	Command filter parameters	
	ζ_{cf}	ω_{cf} (rad/s)
x_{3c}^0, x_{4c}^0	1	10
x_{5c}^0, x_{6c}^0	1	160
$u_{\theta c}^0, u_{\phi c}^0$	1	180

Fig. 6. Saturated acceleration command in azimuth loop in case 1.
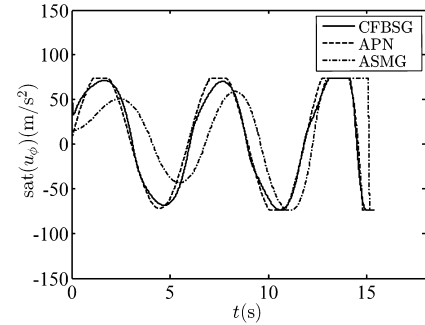

Fig. 7. Saturated acceleration command in elevation loop in case 1.

To demonstrate the effectiveness of the CFBSG, the augmented proportional navigation (APN) guidance law [28] and the adaptive sliding-mode guidance law (ASMG) [32] are introduced for comparison. The APN and ASMG are given by $u_\theta = -3.5\dot{r}\dot{\theta} + a_{T\theta}$, $u_\phi = -3.5\dot{r}\dot{\phi} + a_{T\phi}$ and $u_\theta = -3.5\dot{r}\dot{\theta} + 100\dot{\theta}/(|\dot{\theta}| + 0.01)$, $u_\phi = -3.5\dot{r}\dot{\phi} + 100\dot{\phi}/(|\dot{\phi}| + 0.01)$, respectively, where the target accelerations $a_{T\theta}$ and $a_{T\phi}$ are assumed to be exactly known. The parameters of the CFBSG are set as $\varepsilon_1 = \varepsilon_2 = 100$, $k_1 = k_2 = 0.5$, $k_3 = k_4 = 1$, $k_5 = k_6 = 1.5$, $\zeta = 0.28$, and $\omega_n = 2$. The command filter parameters are given in Table 1. To attenuate chattering, the sign function sgn$x$ in the CFBSG is replaced with a continuous function $x/(|x| + \delta)$, where δ is set to be 0.001.

Case 1: Deterministic case where measurement noise is not considered.

In this case, the saturated acceleration command in azimuth loop and that in elevation loop are plotted in Figs. 6 and 7, respectively. The LOS angular rate in azimuth loop and that in elevation loop are plotted in Figs. 8 and 9, respectively. The eventual flight path in xz plane and that in xy plane are plotted in Figs. 10 and 11, respectively. The missed distances under different guidance laws are listed in Table 2.

Figs. 6 and 7 indicate that the acceleration commands under the CFBSG experience the occurrence of saturation to some extent. Figs. 8 and 9 illustrate that under the CFBSG, the LOS angular rates are restricted in a small neighborhood around zero and finally they deteriorate due to the occurrence of acceleration command saturation. But the thorough divergence of the LOS angular rates occurs at the last instant of interception, indicating that the guidance pre-
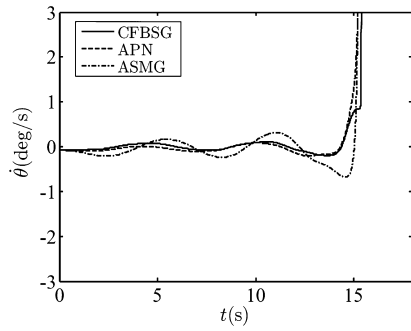
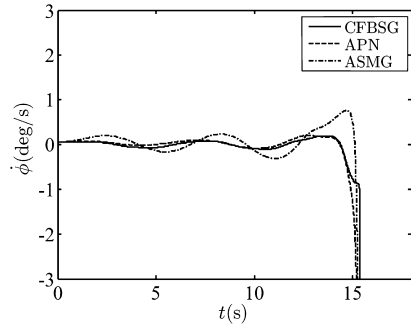**Fig. 8.** LOS azimuth angular rate in case 1.

Fig. 9. LOS elevation angular rate in case 1.
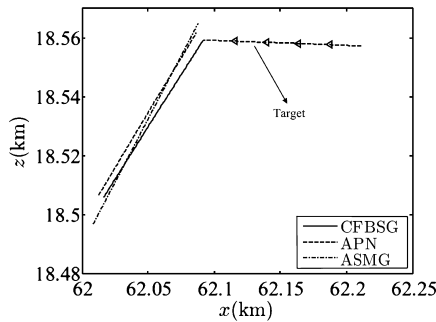

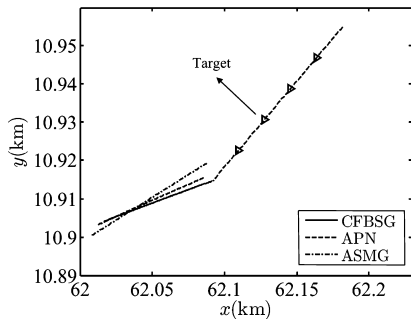**Fig. 10.** Eventual flight path in xz plane in case 1.

Fig. 11. Eventual flight path in xy plane in case 1.

cision is not badly influenced. The successful interception under the CFBSG can be observed from Figs. 10 and 11. The missed distance under the CFBSG is only 0.03 m, which can be seen from Table 2.

In contrast, the LOS angular rates under the APN and ASMG diverge a little earlier (see Figs. 8 and 9) due to the harmful influence of acceleration command saturation (see Figs. 6 and 7) and the delay to guidance command due to the dynamics of missile autopilot. Thus much larger miss distances are yielded under the

Table 2
Summary of miss distances.

Guidance law	Miss distance in case 1 (m)	Averaged miss distance in case 2 (m)
CFBSG	0.03	0.42
APN	4.76	4.76
ASMG	6.58	6.46

Table 3
Distribution of the miss distances in case 2.

Guidance law	Distribution of miss distances (m)			
	≤ 0.3	≤ 0.5	≤ 1.0	≤ 1.5
CFBSG	48%	71%	94%	100%

APN and ASMG (see Table 2). The APN outperforms the ASMG a little because it exactly knows the target acceleration information.

Case 2: Stochastic case where measurement noise is considered.

Here, we will investigate the performance of the proposed CF-BSG in stochastic case where measurement noise is considered. Assume that the LOS angular rates measured by a seeker contain white noise with power spectral density (PSD) of 0.00015 rad/s and the measurements of the gyroscope and accelerometer also contains white noise with PSD of 0.0001 rad/s and 0.0001 m/s^2, respectively. The figures through one time of simulation are not plotted because they are similar with those in case 1 and only some "burrs" appear in the acceleration commands and LOS angular rates. Then 100 times of Monte-Carlo simulations are carried out and the resultant averaged miss distances under the CFBSG, APN, and ASMG are 0.42 m, 4.76 m, and 6.46 m, respectively, also listed in Table 2. Additionally, the distribution of the miss distances under the CFBSG is presented in Table 3, revealing that the probability of miss distance less than 1 m reaches 94%, a very high level.

5. Conclusions

This paper has been concerned with the problem of designing a three-dimensional nonlinear guidance law accounting for both acceleration command saturation and second-order dynamics of the missile autopilot. The guidance law is derived based on CFBS scheme. In the design, the time derivatives of the virtual controls are obtained by filtering, which removes the complexity of analytic calculation. The acceleration command saturation is addressed with the combination of command filters and extra auxiliary filters. Simulation results show that the proposed guidance law is able to provide an excellent guidance precision even though subject to missile acceleration saturation constraint and time delay of actual missile autopilot.

Conflict of interest statement

We confirm that there are no conflicts of interest associated with this publication.

Acknowledgements

References

[1] S. Bezick, I. Rusnak, W.S. Gray, Guidance of a homing missile via nonlinear geometric control methods, J. Guid. Control Dyn. 18 (3) (1995) 441–448.
[2] D.Y. Chwa, J.Y. Choi, Adaptive nonlinear guidance law considering control loop dynamics, IEEE Trans. Aerosp. Electron. Syst. 39 (4) (2003) 1134–1143.
[3] J. Farrell, M. Polycarpou, M. Sharma, On-line approximation based control of uncertain nonlinear system, in: Proceedings of the 2004 American Control Conference, Boston, Massachusetts, USA, 2004, pp. 2557–2562.

[4] J. Farrell, M. Sharma, M. Polycarpou, Backstepping-based flight control with adaptive function approximation, J. Guid. Control Dyn. 28 (6) (2005) 1089–1101.

[5] M. Golestani, I. Mohammdzaman, A.R. Vali, Finite-time convergent guidance law based on integral backstepping control, Aerosp. Sci. Technol. 39 (2014) 370–376.

[6] G. Hexner, A.W. Pila, Practical stochastic optimal guidance law for bounded acceleration missiles, J. Guid. Control Dyn. 34 (2) (2011) 437–445.

[7] G. Hexner, T. Shima, Stochastic optimal control guidance law with bounded acceleration, IEEE Trans. Aerosp. Electron. Syst. 43 (1) (2007) 71–78.

[8] G. Hexner, T. Shima, H. Weiss, LQG guidance law with bounded acceleration command, IEEE Trans. Aerosp. Electron. Syst. 44 (1) (2008) 77–86.

[9] G. Hexner, H. Weiss, Stochastic approach to optimal guidance with uncertain intercept time, IEEE Trans. Aerosp. Electron. Syst. 46 (4) (2010) 1804–1820.

[10] B. Kada, Arbitrary-order sliding-mode-based homing-missile guidance for intercepting highly maneuverable targets, J. Guid. Control Dyn. 37 (6) (2014) 1999–2013.

[11] H.K. Khalil, Nonlinear Systems, third ed., Prentice-Hall, New Jersey, 2002.

[12] N. Lechevin, C.A. Rabbath, Lyapunov-based nonlinear missile guidance, J. Guid. Control Dyn. 27 (6) (2004) 1096–1102.

[13] Y.W. Liang, C.C. Chen, D.C. Liaw, et al., Robust guidance law via integral-sliding-mode scheme, J. Guid. Control Dyn. 37 (3) (2014) 1038–1041.

[14] J. Moon, K. Kim, Y. Kim, Design of missile guidance law via variable structure control, J. Guid. Control Dyn. 24 (4) (2001) 659–664.

[15] I. Rusnak, Advanced guidance laws for acceleration constrained missile, randomly maneuvering target and noisy measurements, IEEE Trans. Aerosp. Electron. Syst. 32 (1) (1996) 456–464.

[16] I. Rusnak, L. Meir, Modern guidance law for high-order autopilot, J. Guid. Control Dyn. 14 (5) (1990) 1056–1058.

[17] I. Rusnak, L. Meir, Optimal guidance for acceleration constrained missile and maneuvering target, IEEE Trans. Aerosp. Electron. Syst. 26 (4) (1990) 618–624.

[18] I. Rusnak, L. Meir, Optimal guidance for high order and acceleration constrained missile, J. Guid. Control Dyn. 14 (3) (1991) 589–596.

[19] T. Shima, O.M. Golan, Linear quadratic differential games guidance law for dual controlled missiles, IEEE Trans. Aerosp. Electron. Syst. 43 (3) (2007) 834–842.

[20] S.H. Song, I.J. Ha, A Lyapunov-like approach to performance analysis of 3-dimensional pure PNG laws, IEEE Trans. Aerosp. Electron. Syst. 30 (1) (1994) 238–247.

[21] L. Sonneveldt, Q.P. Chu, J.A. Mulder, Nonlinear flight control design using constrained adaptive backstepping, J. Guid. Control Dyn. 30 (2) (2007) 322–336.

[22] R. Steve, Missile guidance comparison, in: AIAA Guidance, Navigation, and Control Conference and Exhibit, 2004.

[23] S. Sun, D. Zhou, W.T. Hou, A guidance law with finite time convergence accounting for autopilot lag, Aerosp. Sci. Technol. 25 (2013) 132–137.

[24] C.D. Yang, H.Y. Chen, Nonlinear H_∞ robust guidance law for homing missiles, J. Guid. Control Dyn. 21 (6) (1998) 882–890.

[25] C.D. Yang, H.Y. Chen, Three-dimensional nonlinear H_∞ guidance law, Int. J. Robust Nonlinear Control 11 (2001) 109–129.

[26] R.T. Yanushevsky, Concerning Lyapunov-based guidance, J. Guid. Control Dyn. 29 (2) (2006) 509–511.

[27] J.K. Ye, H.M. Lei, D.F. Xue, et al., Nonlinear differential geometric guidance for maneuvering target, J. Syst. Eng. Electron. 23 (5) (2012) 752–760.

[28] P. Zarchan, Tactical and Strategic Missile Guidance, third ed., AIAA, Washington, 2007.

[29] P. Zhang, Y.W. Fang, F.M. Zhang, et al., An adaptive weighted differential game guidance law, Chin. J. Aeronaut. 25 (2012) 739–746.

[30] Z.X. Zhang, S.H. Li, S. Luo, Terminal guidance laws of missile based on ISMC and NDOB with impact angle constraint, Aerosp. Sci. Technol. 31 (2013) 30–41.

[31] D. Zhou, C.D. Mu, T.L. Shen, Robust guidance law with L_2 gain performance, Trans. Jpn. Soc. Aeronaut. Space Sci. 44 (144) (2001) 82–88.

[32] D. Zhou, C.D. Mu, W.L. Xu, Adaptive sliding-mode guidance of a homing missile, J. Guid. Control Dyn. 22 (4) (1999) 584–589.

[33] D. Zhou, P.P. Qu, S. Sun, A guidance law with terminal impact angle constraint accounting for missile autopilot, J. Dyn. Syst. Meas. Control, Trans. ASME 135 (2013).